NEW RESONANCE CROSS SECTION CALCULATIONAL ALGORITHMS *

by
Donald R. Mathews
General Atomic Co.
P.O. Box 81608
San Diego, Calif. 92138

Improved resonance cross section calculational algorithms have been developed and tested for inclusion in a fast reactor version of the MICROX code[1]. The resonance energy portion of the MICROX code solves the neutron slowing down equations for a two region lattice cell on a very detailed energy grid (about 14500 energies). In the MICROX algorithms, the exact P_0 elastic scattering kernels are replaced by synthetic (approximate) elastic scattering kernels which permit the use of an efficient and numerically stable recursion relation solution of the slowing down equations. In the work described here, the MICROX algorithms have been modified to include:

1. An additional delta function term in the P_0 synthetic scattering kernel per a suggestion by Turinsky and Roman [2]. The additional delta function term allows one more moment of the exact elastic scattering kernel to be preserved without much extra computational effort. With the improved synthetic scattering kernel, the flux returns more closely to the exact flux below a resonance than with the original MICROX kernel.

2. The slowing down calculation has been extended to a true B_1 hyper-fine energy grid calculation in each region using P_1 synthetic scattering kernels and transport-corrected P_0 collision probabilities to couple the two regions.

* Work Supported by the Department of Energy, Contract EY-76-C-03-0167.

1. INTRODUCTION:

The algorithms described here have been incorporated into a new code called SKM2. The SKM2 code is effectively a modernized GAROL code[3].

The original version of the SKM code was written by P. Walti as part of the development of the MICROX code[1]. The SKM code solved the neutron slowing down equations for a two-region lattice cell on a very detailed energy grid in the resonance energy region. Spatially flat and isotropic neutron emission densities in each region were assumed for evaluating the P_0 collision probabilities used to couple the fluxes in the two region cell. A second level of heterogeneity was also treated, i.e., one region could have imbedded grains(particles). The effect of neutron leakage was approximated by the addition of a DB^2 absorption term. The input cross sections were read from a 9000 energy ($\Delta u = 0.001$) GAR data tape[4] prepared by the GAND code[5]. Isotropic in the center of mass coordinate system P_0 elastic scattering was assumed for the neutron slowing down process. The exact elastic scattering kernels were replaced by synthetic (approximate) elastic scattering kernels which permitted a very rapid evaluation of the slowing down integrals via an efficient and numerically stable recursion relation.

The development of a more accurate synthetic scattering kernel, extension to true B_1 calculation in each region, and results for an HTGR test problem follow.

2. NEW SYNTHETIC SCATTERING KERNEL ALGORITHMS

2.1 Exact Elastic Scattering Kernels

The $\ell=0(P_o)$ Legendre moment of the exact isotropic in the center-of-the mass coordinate system elastic scattering kernel is

$$P_o(u\to u') = \frac{\theta(u'-u)\theta(q-u'+u)}{1-\alpha} e^{-(u'-u)} \tag{2.1}$$

where

$$\alpha \equiv \left(\frac{A-1}{A+1}\right)^2 \tag{2.2}$$

$$q \equiv -\ell n\ \alpha \tag{2.3}$$

$$\theta(x) \equiv \begin{cases} 1 \text{ for } x \geq 0 \\ 0 \text{ for } x < 0 \end{cases} \tag{2.4}$$

and A is the atomic mass of the nuclide in question (in units of the mass of the neutron). Equation (2.1) is identifiable as isotropic in the center-of-mass system neutron scatter from a zero temperature free gas. The $\ell=1(P_1)$ Legendre moment of the exact kernel is

$$P_1(u\to u') = \frac{\theta(u'-u)\theta(q-u'+u)}{2(1-\alpha)} \left[(A+1)e^{-(3/2)(u'-u)} - (A-1)e^{-(1/2)(u'-u)}\right] \tag{2.5}$$

2.2 Lethargy Moments of the Exact Kernels

The n^{th} lethargy moment of a scattering kernel will be defined here as

$$I_\ell^{(n)} \equiv \int_u^\infty (u'-u)^n P_\ell(u\to u')du'. \tag{2.6}$$

Analytic expressions for the n = 0, 1, 2 lethargy moments of the exact P_o and P_1 elastic scattering kernels are given in Table 1.

TABLE 1

Lethargy Moments of the Exact Elastic Scattering Kernels

QUANTITY	$A \neq 1$	$A = 1$	$A \gg 1$
$I_0^{(0)}$	1	1	1
$I_0^{(1)}$	$1 + \frac{\alpha}{1-\alpha}\ell n\alpha$	1	$\frac{2}{A}$
$I_0^{(2)}$	$2 + \frac{\alpha}{1-\alpha}\ell n\alpha(2-\ell n\alpha)$	2	$\frac{16}{3A^2}$
$I_1^{(0)}$	$\frac{2}{3A}$	$\frac{2}{3}$	$\frac{2}{3A}$
$I_1^{(1)}$	$-\frac{(A-1)^2(A+2)}{6 \cdot A}\ell n\alpha + \frac{10}{9 \cdot A} - \frac{2 \cdot A}{3}$	$\frac{4}{9}$	$-\frac{2}{3A}$
$I_1^{(2)}$	$\frac{(A-1)^2(A+2)}{6 \cdot A}(\ell n\alpha)^2 - \frac{2(A-1)^2(4A+5)}{9 \cdot A}\ell n\alpha - \frac{32 \cdot A}{9} + \frac{112}{27 \cdot A}$	$\frac{16}{27}$	$-\frac{8}{3A^2}$

2.3 Revised Synthetic Scattering Kernels

The Turinsky-Roman synthetic scattering kernel is[2]

$$p(u\to u') = \theta(u'-u)\left[f\cdot\delta(u'-u) + \text{Real}\left\{ghe^{-g(u'-u)}\right\}\right] \qquad (2.7)$$

where the constants f, g and h depend upon the nuclide mass A but not upon lethargy. Note that g and h are complex.

Wälti's synthetic scattering kernel has the same form as the Turinsky-Roman kernel except that the real constant f in Eq. (2.6) is taken to be zero (no delta function term).

In the SKM2 code, the P_o and P_1 synthetic scattering kernels are both assumed to be of the functional form of Eq. (2.6). Only the numerical values of the constants differ between the P_o and P_1 kernels. The subscript denoting the Legendre moment index will be omitted in the following discussion to simplify the notation.

The values of the constants appearing in Eq. (2.6) are determined in the same manner as in the original Wälti derivation[1] except that one more lethargy moment of the exact scattering kernel may now be matched by the synthetic kernel because of the extra delta function term.

Using Eq. (2.7) in Eq. (2.6) yields the following expression for the lethargy moments of the Turinsky-Roman synthetic scattering kernel

$$I^{(o)} = f + h_r \qquad (2.8)$$

$$I^{(1)} = \frac{h_r g_r + h_i g_i}{g_r^2 + g_i^2} \qquad (2.9)$$

$$I^{(2)} = \frac{2h_r(g_r^2 - g_i^2) + 4h_i g_r g_i}{(g_r^2 + g_i^2)^2} \qquad (2.10)$$

where the r and i subscripts denote the real and imaginary parts of g and h, respectively.

After equating Eqs. (2.8) through (2.10) to the expressions for the lethargy moments of the exact kernels given previously, we now have three equations for the determination of 5 unknowns (f, g_r, g_i, h_r and h_i).

Following Wälti, the values of g_r and g_i are obtained from a least squares fit of the synthetic kernel to the exact kernel. This means that

$$\varepsilon^2(u) = \int_u^\infty \left\{ \text{Real}\left[g h e^{-g(u'-u)} \right] - p^{\text{exact}}(u \to u') \right\}^2 du' \qquad (2.11)$$

should be minimized with respect to g. The P_o results obtained by Wälti for this minimization problem were expressed in the approximate forms

$$g_r = \begin{cases} 1 & \text{for } A=1 \\ (1.10 - 0.50/A)/I_o^{(1)} & \text{for } A \geq 2 \end{cases} \qquad (2.12)$$

$$g_i = \begin{cases} 0 & \text{for } A=1 \\ (1.64 - 0.24/(A-1.2))/q & \text{for } A \geq 2. \end{cases} \qquad (2.13)$$

The P_1 results obtained by Wälti were that the P_1 values of g_r and g_i may be assumed to be the same as the P_o values for $A \geq 2$ and that $g_r = 3/2$, $g_i = 0$ for $A=1$. Note that the P_o and P_1 synthetic kernels are exact for $A=1$ (hydrogen).

For given values of g_r and g_i obtained from the least squares fitting process, Eqs. (2.9) and (2.10) may be solved for h_r and h_i in the forms

$$h_r = 2g_r I^{(1)} - (1/2)(g_r^2 + g_i^2) I^{(2)} \qquad (2.14)$$

$$h_i = \begin{cases} 0 & \text{for } A=1 \\ \left[-(g_r^2 - g_i^2) I^{(1)} + (1/2) g_r (g_r^2 + g_i^2) I^{(2)} \right] / g_i & \text{for } A \geq 2 \end{cases} \qquad (2.15)$$

following which Eq. (2.8) yields

$$f = I^{(o)} - h_r. \qquad (2.16)$$

Turinsky and Roman chose to perform the minimization of Eq. (2.11) with respect to h rather than g. This approach leads to somewhat more complicated expressions for the various constants which they solved by

an iterative scheme. Wälti's approach seems preferable on physical grounds. The constant g appears in an exponential and contains the main information about the shape of the synthetic kernel whereas the constant h is primarily a normalization factor. It therefore seems more appropriate to perform the least squares fit to the exact kernel in terms of the "shape" parameter g rather than the "amplitude" parameter h.

Results obtained with the SKM2 code are thus not precisely comparable to those obtained by Turinsky and Roman because of differences in the method of choosing the synthetic kernel parameters even though in both schemes the 0^{th} through 2^{nd} lethargy moments of the exact kernel are preserved along with a least squares fit to the exact kernel.

2.4 Revised Slowing Down Source Recursion

Let the Turinsky-Roman synthetic scattering kernel be represented by

$$p(u) = f\cdot\delta(u) + \theta(u)\ \text{Real}\left[ghe^{-gu}\right] \tag{2.17}$$

where

$$\theta(u) = \begin{cases} 1 \text{ for } u\geq 0 \\ 0 \text{ for } u<0 \ . \end{cases} \tag{2.18}$$

The complex slowing down source to a given lethargy u is

$$H(u) = \int_{-\infty}^{u} F(u') \left[f\cdot\delta(u-u') + ghe^{-g(u-u')}\right] du' \tag{2.19}$$

or

$$H(u) = f\cdot F(u) + \int_{-\infty}^{u} F(u')\ ghe^{-g(u-u')}du' \tag{2.20}$$

where

$$F(u') \equiv \phi(u')\Sigma_s(u') \ . \tag{2.21}$$

Similarly

$$H(u+\Delta) = f\cdot F(u+\Delta) + \int_{-\infty}^{u+\Delta} F(u')ghe^{-g(u+\Delta-u')}du' \tag{2.22}$$

or

$$H(u+\Delta)=f\cdot F(u+\Delta)+e^{-g\Delta}\int_{-\infty}^{u} F(u')ghe^{-g(u-u')}du'+\int_{0}^{\Delta}F(u+\Delta-v)ghe^{-gv}dv \tag{2.23}$$

where

$$v \equiv u+\Delta-u' . \tag{2.24}$$

Using Eq. (2.20) in Eq. (2.23) yields

$$H(u+\Delta) = f\cdot F(u+\Delta) + e^{-g\Delta}\left[H(u)-f\cdot F(u)\right] + \int_0^{\Delta} F(u+\Delta-v)\,ghe^{-gv}dv \tag{2.25}$$

Let the scattering density F(u) be represented by a linear function of u in the interval of u to u+Δ, i.e., let

$$F(u') = a + bu' \tag{2.26}$$

or

$$F(u+\Delta-v) = F(u+\Delta) + \left[F(u) - F(u+\Delta)\right]\left(\frac{v}{\Delta}\right) \tag{2.27}$$

With this assumption the last integral in Eq. (2.25) becomes

$$\int_0^{\Delta} F(u+\Delta-v)\,ghe^{-gv}dv = F(u+\Delta)h\left[1-\left(\frac{1-e^{-g\Delta}}{g\Delta}\right)\right] + F(u)\,h\left[\left(\frac{1-e^{-g\Delta}}{g\Delta}\right)-e^{-g\Delta}\right] \tag{2.28}$$

Now define

$$A(g\Delta) \equiv 1-\left(\frac{1-e^{-g\Delta}}{g\Delta}\right) \tag{2.29}$$

and

$$B(g\Delta) \equiv \left(\frac{1-e^{-g\Delta}}{g\Delta}\right)-e^{-g\Delta} \tag{2.30}$$

so that Eq. (2.28) becomes

$$H(u+\Delta)=e^{-g\Delta}\cdot H(u)+F(u)\left[B(g\Delta)h-f\cdot e^{-g\Delta}\right] + F(u+\Delta)\left[A(g\Delta)h+f\right] . \tag{2.31}$$

To obtain a recursion similar to Wälti's, set

$$\hat{A}(g\Delta)\equiv A(g\Delta)h+f \tag{2.32}$$

and

$$\hat{B}(g\Delta) \equiv B(g\Delta)h - f\cdot e^{-g\Delta} \tag{2.33}$$

to obtain

$$H(u+\Delta)=e^{-g\Delta}H(u) + \hat{B}(g\Delta)\cdot F(u) + \hat{A}(g\Delta)\cdot F(u+\Delta). \tag{2.34}$$

For the real part of $(q\Delta) < 0.05$, the following series expansions are used in the SKIP code

$$e^{-g\Delta} \cong 1-g\Delta(1-g\Delta((1/2) - g\Delta((1/6) - (1/24)\,g\Delta))) \tag{2.35}$$

$$A(g\Delta) \cong g\Delta(1/2) - g\Delta((1/6) - g\Delta((1/24) - (1/120)\,g\Delta))) \tag{2.36}$$

$$B(g\Delta) \cong g\Delta((1/2) - g\Delta((1/3) - g\Delta((1/8) - (1/30)\,g\Delta))) \tag{2.37}$$

3. POINTWISE B_1 EQUATIONS

3.1 N-Region B_1 Equations

The B_1 equations used by the SKM2 Code were derived from the B_1 equations for a single region given in Ref. 4 by assuming P_o collision probability coupling* between regions as in the MICROX code[1]. The B_1 equations for the j^{th} of N regions may then be written in the form

$$|B|\varphi_{1j}(u) + \Sigma_{tj}(u)\varphi_{oj}(u) = \frac{1}{V_j}\sum_{i=1}^{N} V_i P_{ij}(u)\, S_{oi}(u) \qquad (3.1.a)$$

$$3\gamma_j(u)\,\Sigma_{tj}(u)\varphi_{1j}(u) - \frac{B^2}{|B|}\,\varphi_{oj}(u) = 3S_{1j}(u) \qquad (3.1.b)$$

where

$$S_{\ell j}(u) \equiv \int_{-\infty}^{u} \varphi_{\ell j}(u')\,\Sigma_{sj}(u')P_{\ell j}(u-u')du' + S^{ex}_{\ell j}(u) \qquad (3.2)$$

$$\gamma_j(u) \equiv \frac{X_j}{3\left[R(X_j)-1\right]} \qquad (3.3)$$

$$X_j \equiv \frac{B^2(u)}{\Sigma^2_{tj}(u)} \qquad (3.4)$$

$$y_j \equiv \sqrt{|X_j|} \qquad (3.5)$$

---

* The effect of anisotropic (P_1) scattering effects on the region couplings are approximated by replacing the total cross section by the transport cross section during the evaluation of the collision probabilities.[6,7,8] This refinement was used only in the thermal section of the MICROX code[1]. Except for this change, the SKM2 code uses the collision probability calculational algorithms described in Ref. 1.

$$R(X_j) \equiv \begin{cases} \dfrac{y_j}{\tan^{-1} y_j} & \text{for } X_j > 0 \\ \dfrac{y}{\tanh^{-1} y_j} & \text{for } X_j < 0 \end{cases} \tag{3.6}$$

For $|X_j| < 0.25$

$$\gamma_j(u) = 1 + \frac{\frac{4}{15} X_j - \frac{8}{35} X_j^2 + \frac{4}{21} X_j^3}{1 - \frac{3}{5} X_j + \frac{3}{7} X_j^2 - \frac{1}{3} X_j^3} \tag{3.7}$$

Using (3.2) in (3.1.a) and (3.1.b) and dropping references to the lethargy u at which the fluxes are being computed yields

$$|B|\phi_{1j} + \Sigma_{tj}\phi_{oj} = \sum_{i=1}^{N} \frac{V_i}{V_j} P_{ij} \left\{ \int_{-\infty}^{u} \phi_{oi}(u')\Sigma_{si}(u')p_{oi}(u-u')du' + S_{oi}^{ex} \right\} \tag{3.8.a}$$

$$\gamma_j \Sigma_{tj}\phi_{1j} - \frac{1}{3}\frac{B^2}{|B|}\phi_{oj} = \int_{-\infty}^{u} \phi_{1j}(u')\Sigma_{sj}(u')P_{1j}(u-u')du' + S_{1j}^{ex} \tag{3.8.b}$$

Now define the scattering kernels to be approximate (synthetic) kernels of the Turinsky-Roman form discussed previously, i.e.,

$$P_{\ell j}(u) \equiv f_{\ell j}\cdot\delta(u) + \vartheta(u)\cdot \text{Real}\left[g_{\ell j} h_{\ell j} e^{-g_{\ell j}\cdot u}\right] \tag{3.9}$$

where the $f_{\ell j}$ are real constants, $\delta(u)$ is the Dirac delta function, $\vartheta(u)$ is the Heaviside function defined by

$$\vartheta(u) = \begin{cases} 1 \text{ for } u > 0 \\ 0 \text{ for } u < 0 \end{cases} \tag{3.10}$$

and the $g_{\ell j}$ and $h_{\ell j}$ are complex constants. Further define the complex slowing down sources

$$H_{\ell j}(u) \equiv \phi_{\ell j}(u)\Sigma_{sj}(u)f_{\ell j} + g_{\ell j}h_{\ell j}\int_{-\infty}^{u}\phi_{\ell j}(u')\Sigma_{sj}(u')e^{-g_{\ell j}(u-u')}du' \tag{3.11}$$

and now that

$$S_{\ell j}(u) = \text{Real}\left[H_{\ell j}(u)\right] + S^{ex}_{\ell j}(u) \tag{3.12}$$

As shown in the previous section, the $H_{\ell j}(u)$ obey the following recursion relation

$$H_{\ell j}(u+\Delta) = e^{-g_{\ell j}\Delta}H_{\ell j}(u) + D_{\ell j}\phi_{\ell j}(u) + A_{\ell j}\phi_{\ell j}(u+\Delta) \tag{3.13}$$

where

$$D_{\ell j} \equiv \Sigma_{sj}(u)\left\{h_{\ell j}\left[\frac{1-e^{-g_{\ell j}\Delta}}{g_{\ell j}\Delta} - e^{-g_{\ell j}\Delta}\right] - f_{\ell j}e^{-g_{\ell j}\Delta}\right\} \tag{3.14}$$

$$A_{\ell j} \equiv \Sigma_{sj}(u+\Delta)\left\{h_{\ell j}\left[1 - \frac{1-e^{-g_{\ell j}\Delta}}{g_{\ell j}\Delta}\right] + f_{\ell j}\right\} \tag{3.15}$$

If we further define

$$C_{\ell j} \equiv D_{\ell j}\phi_{\ell j}(u) + e^{-g_{\ell j}\Delta}H_{\ell j}(u) \tag{3.16}$$

then Eq. (3.13) becomes

$$H_{\ell j}(u+\Delta) = A_{\ell j}\phi_{\ell j}(u+\Delta) + C_{\ell j} \tag{3.17}$$

Using the above definitions in Eqs. (3.8.a) and (3.8.b) yields

$$|B|\phi_{1j} + \Sigma_{tj}\phi_{oj} = \sum_{i=1}^{N}\frac{V_i}{V_j}P_{ij}\left\{\text{Real}\left[H_{oi}(u)\right] + S^{ex}_{oi}\right\} \tag{3.18.a}$$

$$\gamma_j\Sigma_{tj}\phi_{1j} - \frac{1}{3}\frac{B^2}{|B|}\phi_{oj} = \text{Real}\left[H_{1j}(u)\right] + S^{ex}_{1j} \tag{3.18.b}$$

Rewriting Eqs. (3.18.a) and (3.18.b) at $u+\Delta$ and using Eq. (3.17) yields

$$|B(u+\Delta)|\phi_{ij}(u+\Delta)+\Sigma_{tj}(u+\Delta)\phi_{oj}(u+\Delta) = \sum_{i=1}^{N}\frac{V_i}{V_j}P_{ij}\left\{\phi_{oi}(u+\Delta)\text{Real}\left[A_{oi}\right] + \text{Real}\left[C_{oi}\right] + S^{ex}_{oi}(u+\Delta)\right\} \tag{3.19.a}$$

$$\gamma_j(u+\Delta)\Sigma_{tj}(u+\Delta)\phi_{1j}(u+\Delta) - \frac{1}{3}\frac{B^2(u+\Delta)}{|B(u+\Delta)|}\phi_{oj}(u+\Delta)=\phi_{1j}(u+\Delta)\text{Real}\left[A_{1j}\right]$$
$$+\text{Real}\left[C_{1j}\right]+ S_{1j}^{ex}(u+\Delta) \qquad (3.19.b)$$

Collecting terms and dropping references to u+Δ

$$|B|\phi_{1j} + \left\{\Sigma_{tj} - P_{jj}\text{Re}\ (A_{oj})\right\}\phi_{oj} - \sum_{i\neq j}\frac{V_i}{V_j}P_{ij}\phi_{oi}\text{Re}(A_{oi}) =$$

$$\sum_{i=1}^{N}\frac{V_i}{V_j}P_{ij}\left\{\text{Re}(C_{oi}) + S_{oi}^{ex}\right\} \qquad (3.20.a)$$

$$\left\{\gamma_j\Sigma_{tj} - \text{Re}(A_{1j})\right\}\phi_{1j} - \frac{1}{3}\frac{B^2}{|B|}\phi_{oj} = \text{Re}(C_{1j}) + S_{1j}^{ex} \qquad (3.20.b)$$

From Eq. (3.20.b) we have

$$|B|\phi_{1j} = \frac{\frac{B^2}{3}\phi_{oj} + |B|\left[\text{Re}(C_{1j}) + S_{1j}^{ex}\right]}{\gamma_j\Sigma_{tj} - \text{Re}\ (A_{1j})} \qquad (3.21)$$

Using Eq. (3.21) in Eq. (3.20.a) yields

$$\left\{\frac{B^2}{3\left[\gamma_j\Sigma_{tj} - \text{Re}(A_{1j})\right]} + \Sigma_{tj} - P_{jj}\text{Re}(A_{oj})\right\}\phi_{oj}$$

$$-\sum_{i\neq j}\frac{V_i}{V_j}P_{ij}\phi_{oi}\text{Re}(A_{oi}) = \qquad (3.22)$$

$$\sum_{i=1}^{N}\frac{V_i}{V_j}P_{ij}\left\{\text{Re}(C_{oi}) + S_{oi}^{ex}\right\} - \frac{|B|\left[\text{Re}(C_{1j})+S_{1j}^{ex}\right]}{\gamma_j\Sigma_{tj} - \text{Re}(A_{1j})}$$

Eq. (3.22) and then (3.21) are the B_1 equations for N regions (j=1, ..., N) coupled by P_o collision probabilities (P_{ij}'s) and using a slowing down source recursion (Eq. 3.16) made possible by assuming approximate separable (synthetic) scattering kernels.

3.2 Two-Region B_1 Equations

Specializing to 2 regions, we have

$$\left\{\frac{B^2}{3[\gamma_1\Sigma_{t1}-\mathrm{Re}(A_{11})]}+\Sigma_{t1}-P_{11}\mathrm{Re}(A_{01})\right\}\phi_{01}-\frac{V_2}{V_1}P_{21}\phi_{02}\mathrm{Re}(A_{02})=Q_{01} \qquad (3.23.a)$$

$$\left\{\frac{B^2}{3[\gamma_2\Sigma_{t2}-\mathrm{Re}(A_{12})]}+\Sigma_{t2}-P_{22}\mathrm{Re}(A_{02})\right\}\phi_{02}-\frac{V_1}{V_2}P_{12}\phi_{01}\mathrm{Re}(A_{01})=Q_{02} \qquad (3.23.b)$$

where

$$Q_{oj}\equiv\sum_{i=1}^{2}\frac{V_i}{V_j}P_{ij}\left\{\mathrm{Re}(C_{oi})+S_{oi}^{ex}\right\}-\frac{|B|\left[\mathrm{Re}(C_{1j})+S_{1j}^{ex}\right]}{\gamma_j\Sigma_{tj}-\mathrm{Re}(A_{1j})} \qquad (3.24)$$

Solving Eqs. (3.23.a) and (3.23.b) for ϕ_{01} and ϕ_{02} yields

$$\phi_{01}=\frac{\left\{\frac{B^2}{3[\gamma_2\Sigma_{t2}-\mathrm{Re}(A_{12})]}+\Sigma_{t2}-P_{22}\mathrm{Re}(A_{02})\right\}Q_{01}+\frac{V_2}{V_1}P_{21}\mathrm{Re}(A_{02})Q_{02}}{E} \qquad (3.25.a)$$

$$\phi_{02}=\frac{\left\{\frac{B^2}{3[\gamma_1\Sigma_{t1}-\mathrm{Re}(A_{11})]}+\Sigma_{t1}-P_{11}\mathrm{Re}(A_{01})\right\}Q_{02}+\frac{V_1}{V_2}P_{12}\mathrm{Re}(A_{01})Q_{01}}{E} \qquad (3.25.b)$$

where

$$E\equiv\left\{\frac{B^2}{3[\gamma_1\Sigma_{t1}-\mathrm{Re}(A_{11})]}+\Sigma_1-P_{11}\mathrm{Re}(A_{01})\right\}\left\{\frac{B^2}{3[\gamma_2\Sigma_{t2}-\mathrm{Re}(A_{12})]}+\Sigma_{t2}-P_{22}\mathrm{Re}(A_{02})\right\}$$

$$-P_{21}\mathrm{Re}(A_{02})P_{12}\mathrm{Re}(A_{01}) \qquad (3.26)$$

4. TEST PROBLEM RESULTS

4.1 Fort St. Vrain HTGR Test Problem

The test problem results presented in this section represent a comparison of selected results from the MICROX code[8], the GGC-5 code[9], the original SKM code and the SKM2 code.

The four-nuclide test problem, which is a simplification of typical Fort St. Vrain reactor problems, is defined by the following data.

Geometry	Cylinder
Diameter of the fuel grains	400 microns
Volume fraction of grains in the rods	0.1027
Diameter of the fuel rods	1.27 cm
Volume fraction of the rods	0.20
Dancoff correction factor	0.42
Buckling	0.0 cm^{-2}
Fission source	U-235
Temperature	1100°K

The broad group energy structure and core composition used for the problem are given in Tables 4.1 and 4.2 respectively.

GGC-5 included a GANDY unresolved resonance calculation for thorium in fine groups 53-63. The value of $\sigma_{m_{eff}}$ was 734 barns and the resonance parameters were chosen so as to reproduce the GAM infinite dilution cross sections.

The GAROL resolved resonance calculation for thorium in GGC-5 (fine groups 64-92) was modified to include the grain-shielding method used in MICROX (Reference *10*) in lieu of the Dyos-Pomraning treatment (Reference *11*).

TABLE 4.1

BROAD GROUP ENERGY STRUCTURE FOR THE
FORT ST. VRAIN HTGR TEST PROBLEM

Broad Group	GAM-II Fine Groups	Lower Energy (eV)
1	1-44	1.832×10^5
2	45-63	3.355×10^3
3	64-68	961.1
4	69-84	17.6
5	85-90	3.928
6	91-92	2.382

TABLE 4.2

CORE COMPOSITION FOR THE FORT ST. VRAIN
HTGR TEST PROBLEM

Nuclide	Density in the Grains [a]	Homogenized Density in the Rod	Homogenized Density in the Moderator	Cell Averaged Density
C	4.41300-2	5.78-2	6.28-2	6.180-2
Th-232	1.94742-2	2.00-3	--	4.000-4
U-235	8.18890-4	8.41-5	--	1.682-5
U-238	4.40117-5	4.52-6	--	9.040-7

a) All densities are in atoms/b-cm.

The MICROX calculation used a reference value of $\Sigma_{tot,2} = 0.2983$ cm^{-1} (macroscopic total cross section in region 2) to correspond to the Dancoff factor of 0.42.

A buckling of 0.0 cm^{-2} was chosen in order to compare GGC-5 and MICROX as closely as possible. In addition, MICROX was run with zero-temperature slowing down in the fast energy range and no thermal upscatter to the fast range was allowed. (The restriction on the thermal upscatter was made because the present version of MICROX always performs a complete calculation including both fast and thermal spectrum computations.)

The cell-averaged microscopic results for the thorium absorption cross sections and the carbon and thorium out-scattering cross sections are compared in Tables 4.3, 4.4, and 4.5, respectively. The GGC-5, GAROL and MICROX results are from Ref. 1.

The major thorium resonances are located in broad group 4 in these calculations. The group 4 thorium absorption cross section is 0.72% higher than the SKM or MICROX results. The change in the group 4 thorium absorption cross section between the SKM and SKM2 codes is due to the following effects:

1. A 1.05% decrease due to the improved synthetic scattering kernel in the SKM2 code.
2. A 1.49% increase due to the use of the transport cross section instead of the total cross section in the computation of the regionwise collision probabilities in the SKM2 code.
3. A 0.18% increase due to the use of the transport cross section in the computation of the grain shielding.

TABLE 4.3

THORIUM ABSORPTION CROSS SECTIONS FOR THE FORT ST. VRAIN HTGR TEST PROBLEM

Group	GGC-5	GAROL	MICROX	SKM	SKM2
1	0.1712	--	0.1712	--	--
2	0.6332	--	0.6357	--	--
3	1.7730	1.7731	1.7986	1.7727	1.7723
4	7.8354	7.8664	7.8556	7.8555*	7.9120
5	0.1393	0.1393	0.1393	0.1393	0.1393
6	0.2963	0.2962	0.2962	0.2962	0.2962

* 7.8636 with built-in point skipping criteria.

TABLE 4.4

Carbon P_0 Outscattering Cross Sections For The Fort St. Vrain HTGR Test Problem

Group	GGC-5	MICROX	SKM2
1	0.1986	0.1986	--
2	0.1789	0.1789	--
3	0.5964	0.5953	0.5962
4	0.1511	0.1508	0.1505
5	0.4954	0.4946	0.4948
6	1.5083	1.5046	1.5395

TABLE 4.5

Thorium P_0 Outscatter Cross Sections For the Fort St. Vrain HTGR Test Problem

Group	GGC-5	MICROX	SKM2
1	0.1827	0.1827	--
2	0.0306	0.0306	--
3	0.1148	0.0608	0.0669
4	0.0282	0.0151	0.0151
5	0.0673	0.0618	0.0618
6	0.2072	0.1923	0.1923

It should be noted that item 3 above is included in the present production version of the MICROX code. The results given in Tables 4.3, 4.4, and 4.5 are from the original version of the MICROX code. It is planned to re-run this test problem with the present production version of the MICROX code in the near future. More rigorous tests against the GAROL code with special GAR data tapes using a finer lethargy spacing are also planned.

The effect of the new delta function synthetic scattering kernel on the computed neutron fluxes in the neighborhood of the first two major resonances of thorium is given in Fig. 4.1. As expected, the original Wälti synthetic scattering kernel slightly underestimates the fluxes below the resonances. Insignificant differences in U-235 fission and U-238 capture cross sections were obtained between the SKM and SKM2 codes.

The difference in the results for the carbon out-scattering cross sections between GGC-5 and MICROX is due to the fact that GGC-5 overestimates the effect of out-scattering. The evaluation of GAM cross section data for fine-group out-scattering is based on the assumption that the flux shape within each GAM fine group is flat (constant lethargy flux). In reality, the mean flux at the upper GAM group boundary is greater than the flux at the lower group boundary. A neutron suffering a scattering collision near the lower group boundary is more likely to end up in the next lower GAM group than is a neutron which is scattered near the upper group boundary. Therefore, the GAM out-scattering cross sections are too high. MICROX does not use the constant flux approximation for primary nuclides. The GAROL section of GGC-5 does not suffer from that limitation either; however, the scattering cross sections from GAROL are not presently used by GGC-5 for broad-group averaging.

The reason for the large differences in the results for the thorium out-scattering cross sections is that resonance scattering cross sections are self-shielded in MICROX and SKM2 and unshielded

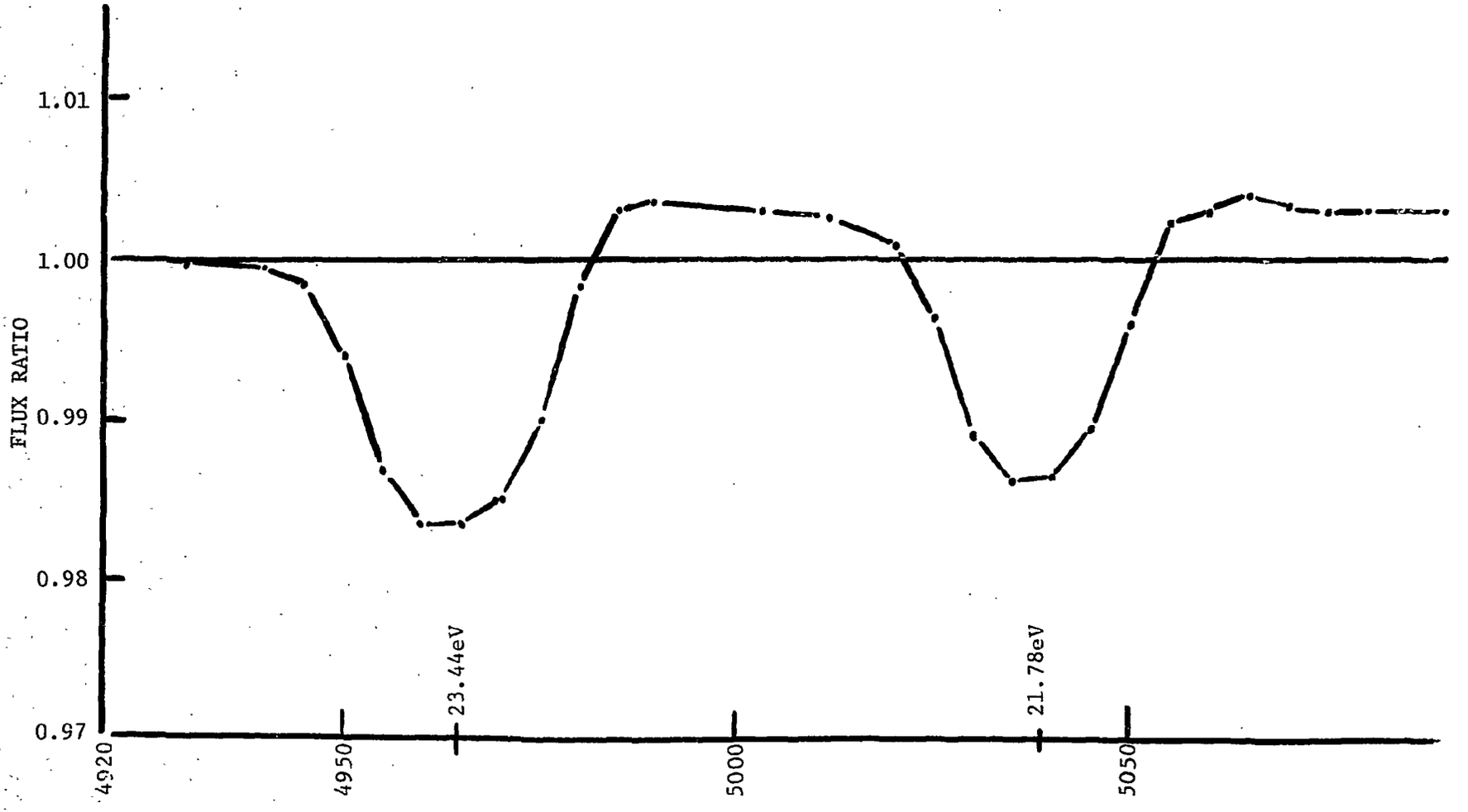

FIG. 4.1 DELTA FUNCTION KERNEL FLUX DIVIDED BY WALTI KERNEL FLUX IN THE THORIUM DOUBLET REGION FOR THE FORT ST. VRAIN HTGR TEST PROBLEM

in GGC-5 except in the internal calculations of the GAROL section. (The thorium out-scattering cross sections are, of course, relatively unimportant in HTGR analysis, but are of considerable importance in fast breeder reactor analyses.)

The SKM code did not compute transfer matrices. The SKM2 code results compare well with the MICROX code results except for the group 6 carbon outscatter. The MICROX code assumption of very wide broad groups breaks down for the relatively narrow group 6.

ACKNOWLEDGEMENTS

R. Moore and W. Davison encouraged this work and provided many helpful comments. P. Koch who worked with P. Wälti on the development of the MICROX code was quite helpful in helping me determine how the original SKM code worked and also contributed many helpful comments on the improvements described here. C. Hamilton provided invaluable moral and financial support.

REFERENCES

1. Walti, P., and P. Koch, "MICROX, A Two-Region Flux Spectrum Code for the Efficient Calculation of Group Cross Sections," Gulf General Atomic Co. Report Gulf-GA-A10827, 1972.

2. Roman, Charles P., "Comparison of Separable Scattering Kernels for Neutron Elastic Slowing Down Theory," M.S. Thesis, Rensselaer Polytechnic Institute, June, 1973.

3. Stevens, C. A., and C. V. Smith, "GAROL, A Computer Program for Evaluating Resonance Absorption Including Resonance Overlap," Gulf General Atomic Report GA-6637, 1965.

4. Archibald, R. J., and D. R. Mathews, "GAFGAR, A Program for the Calculation of Neutron Spectra and Group-Averaged Cross Sections," Gulf General Atomic Inc. Report GA-7542 (vol. I), 1968.

5. Archibald, R. J., and D. R. Mathews, "GAND2 and GFE2, Computer Codes for Preparing Input Data for the GAFGAR, GGC, and MICROX Codes from an ENDF/B Format Nuclear Data File," Gulf General Atomic Co. Report GA-7542 (Vol. II), 1973.

6. Honeck, H. C., "The Calculation of the Thermal Utilization and Disadvantage Factor in Uranium/Water Lattices," Nucl. Sci. & Eng. 18, 49(1969) (see particularly pp. 55-56).

7. Takahashi, H., "The Generalized First-Flight Collision Probability in The Cylindricalized System," Nucl. Sci. & Eng. 24, 69(1966) (see particularly pp. 70-71).

8. Carvik, I., "Calculations of Neutron Flux Distributions by Means of Integral Transport Methods," Report AE-279, 1967 (see particularly pp. 26-27).

9. Mathews, D. R., P. K. Koch, J. Adir, and P. Walti, "GGC-5, A Computer Program for Calculating Neutron Spectra and Group Constants," Gulf General Atomic Co. Report GA-8871, 1971.

10. Walti, P., "Evaluation of Grain Shielding Factors for Coated Fuel Particles," Nucl. Sci. & Eng. 45, 321(1971).

11. Dyos, M. W., and G. C. Pomraning, "Effective Thermal-Neutron Cross Sections for Materials with Grain Structure," Nucl. Sci. & Eng. 25, 8(1966).